Photon scattering by a 4π-spherically-focused ultrastrong electromagnetic wave

Tae Moon Jeong ●,[*] Sergei V. Bulanov,[†] Pavel V. Sasorov ●,[‡] and Georg Korn
Institute of Physics of the ASCR, ELI-Beamlines, Na Slovance 2, 18221 Prague, Czech Republic

James K. Koga ●
Kansai Photon Research Institute, National Institutes for Quantum and Radiological Science and Technology, 8-1-7 Umemidai, Kizugawa-shi, Kyoto 619-0215, Japan

Stepan S. Bulanov
Lawrence Berkeley National Laboratory, Berkeley, California 94720, USA

The scattering of high-power probe laser pulses by tightly focused ultrastrong laser pulses has been investigated through a semiclassical approach using a perturbative method based on the Born approximation. Under a 4π-spherically-focused ultrastrong light field, the electric permittivity and magnetic permeability tensors for vacuum are calculated from the Euler-Heisenberg Lagrangian to show the nonlinear birefringent property of vacuum. And, from permittivity and permeability tensors, the scattering potential is derived for the Born approximation. The first-order solution of the Born approximation is taken as an electric field scattered from the 4π-spherically-focused laser pulse when a probe laser pulse propagates through the focused laser field. The differential cross section of the nonlinear birefringent vacuum is derived, and the number of photons scattered from the nonlinear birefringent vacuum is analyzed in the laser power range of 10–1000 PW.

I. INTRODUCTION

The advance in femtosecond (fs) high-power lasers [1–4] enables one to study laser-plasma interaction in relativistic ($>10^{18}$ W/cm^2) and ultrarelativistic ($>10^{24}$ W/cm^2) regimes [5,6]. And, as the laser intensity approaches the Schwinger limit ($I_{\text{Sch}} \approx 2.3 \times 10^{29}$ W/cm^2) which is even higher than the ultrarelativistic intensity, quantum electrodynamic (QED) features of vacuum come into play and the vacuum behaves like a nonlinear medium, exhibiting vacuum birefringence and electron-positron (e^+e^-) pair production via the Schwinger mechanism [7–10]. These phenomena cannot be treated by classical electrodynamics in which the Lagrangian contains only the E^2-B^2 term. In 1936, Euler and Heisenberg derived a new Lagrangian, known as the Euler-Heisenberg Lagrangian (EH Lagrangian), to describe QED features under high but constant field strength conditions [11]. The EH Lagrangian in the weak field limit where the fields are much less than the Schwinger field can be Taylor-series expanded, successively yielding higher order terms where the first term in the expansion represents light-light scattering [12].

The cross section for light-light scattering was first calculated by Karplus and Neuman using the electrodynamic scattering matrix formalism in QED [13,14], and later De Tollis calculated the light-light scattering through a dispersive approach [15]. Due to the strong attention paid to the nonlinearity of vacuum, much international effort [16–19] has been initiated to detect vacuum birefringence and light-light scattering. However, all these efforts require an ultrastrong field strength to induce vacuum birefringence and to detect light-light scattering. One approach for detecting the light-light scattering is to use high energy photons in the x-ray or γ-ray range [20–22]. These high energy photons can be generated from either conventional accelerators [23] or plasma media interacting with high-power laser pulses [24–26]. When considering the plasma medium, one of the promising ways to obtain such high energy photons is to use a frequency-upshifted laser pulse reflected from a relativistic mirror [27,28]. Thanks to advances in laser technology, other approaches utilizing colliding high-power laser pulses [22,29,30] have been also proposed for light-light scattering.

The ultrastrong field formed by a fs high-power laser pulse might be directly used to investigate the light-light scattering as well. The ultrastrong field strength can be achieved by tightly or spherically focusing fs high-power laser pulses [31–37]. Under the 4π-spherical-focusing scheme, the electric field after a focusing optic reaches the focal spot from almost every direction (i.e., from 4π solid angle) to form a focus. Thus, the 4π-spherical-focusing scheme can be regarded as an extreme case of either multiple laser beam focusing or the tight focusing scheme. According to recent research, the formation of a focused intensity of $\sim10^{27}$ W/cm^2, yielding the field strength of $\sim1.5 \times 10^{15}$ V/cm corresponding to 12% of the Schwinger field, is possible at the focus by spherically

---

[*]taemoon.jeong@eli-beams.eu

[†]Also at Kansai Photon Research Institute, National Institutes for Quantum and Radiological Science and Technology, 8-1-7 Umemidai, Kizugawa-shi, Kyoto 619-0215, Japan.

[‡]Also at Keldysh Institute of Applied Mathematics, Moscow 125047, Russia.

focusing a 100 PW laser pulse with a wavelength of 0.2 μm [37]. As mentioned earlier, such a tightly focused fs high-power laser pulse turns the vacuum into a nonlinear medium with birefringent properties. However, due to the wavelike nature of light, the focused fs high-power laser pulse has a spatiotemporal distribution, so the induced nonlinear birefringent effect of the vacuum becomes dependent on time and space. Therefore, with a fs high-power laser system, the questions, such as how strongly the vacuum nonlinearity is induced by a given laser pulse and how to calculate the scattered E field from the space- and time-dependent nonlinear vacuum, have arisen.

Under the tight focusing condition, Monden and Kodama calculated the number of scattered photons by directly solving Maxwell's equations for a single [38] and two counterpropagating high-power laser pulses [39], in which the QED correction term was introduced through the polarization and magnetization vectors. Since the 4π-spherical-focusing scheme provides the highest attainable laser intensity at a given laser power, other light-light scattering setups using the 4π-spherical-focusing scheme can be considered to maximize scattered photons at a given laser power. In this case, the 4π-spherically-focused laser pulse induces the nonlinearity of vacuum, and an additional probe laser pulse is scattered from the nonlinearity. Under the 4π-spherical-focusing scheme, the vacuum under the ultrastrong field can be treated as a nonlinear birefringent medium of which nonlinearity is induced by a focused laser intensity, and then, instead of directly solving Maxwell's equations, a perturbation method can be applied to solve the light-light scattering problem.

In this paper we investigate the light scattering by an ultrastrong light field obtained by the 4π-spherical-focusing scheme. In order to introduce the nonlinear birefringent behavior to the vacuum, the intensity-dependent electric permittivity and magnetic permeability tensors for vacuum are calculated, through the EH Lagrangian, with the mathematical expressions for the spatiotemporal distribution of an ultrastrong light field which is obtained by 4π-spherically-focusing cylindrical vector (CV) beams [40,41]. A probe laser pulse propagating through a nonlinear birefringent vacuum (NBV) is scattered by a scattering potential expressing the NBV. The scattered field is calculated by a perturbation method using the Born approximation [42]. The scattering properties of the probe laser pulse, such as the differential cross section for scattering and the number of scattered photons, are investigated based on a semiclassical approach.

II. NONLINEAR VACUUM INDUCED BY ULTRASTRONG ELECTROMAGNETIC FIELD

The EH Lagrangian which can describe the light-light scattering is written as [11]

$$L_{\mathrm{EH}} = -\frac{1}{8\pi^2} \int_0^\infty \frac{ds}{s^3} e^{-sm^2} \left[(es)^2 \frac{\mathrm{Re}\cosh(es\sqrt{2(\mathcal{F}+i\mathcal{G})})}{\mathrm{Im}\cosh(es\sqrt{2(\mathcal{F}+i\mathcal{G})})} \mathcal{G} - \frac{2}{3}(es)^2\mathcal{F} - 1 \right]. \tag{1}$$

Here m is the electron mass and e is the electron charge. The Poincaré invariants $\mathcal{F}$ and $\mathcal{G}$ are defined by $(c^2\vec{B}^2 - \vec{E}^2)/2$ and $-c\vec{B}\cdot\vec{E}$, respectively. Although the EH Lagrangian is valid for a constant field, its validity can be extended for a slowly varying field under the locally constant field approximation (LCFA) [43,44], which assumes that the wavelength of the EM wave is much greater than the pair-production length $l_c = mc^2/|eE|$. Since λ (laser wavelength) $\gg l_c$, the LCFA is valid for this study. In the strong-field QED (SF-QED), the validity of the LCFA can be checked by the quantum nonlinearity parameter [45] χ $[\sqrt{|(F^{\mu\nu}p_\nu)^2|}/mcF_{cr}]$, where $F^{\mu\nu}$ is the amplitude of the background field, F_{cr} is the Schwinger field, and p_ν is the initial four momentum of an electron. In this case, the LCFA is valid when $a^3/\chi \gg 1$ [46]. Here a is the normalized vector potential ($|eE|/m\omega c$). Further discussion on the validity of the LCFA in SF-QEDs can be found in [46–50]. The Lagrangian describing the electromagnetic field in vacuum is a sum, $L = L_M + L_{\mathrm{EH}}$, of the classical electrodynamics Lagrangian $L_M = -\epsilon_0 \mathcal{F}$, and of the Euler-Heisenberg Lagrangian L_{EH}. In the weak field limit, the Lagrangian in SI units is expanded as

$$L \approx \frac{\epsilon_0}{2}(\vec{E}^2 - \delta\vec{H}^2) + \frac{\epsilon_0\kappa}{2}[(\vec{E}^2 - \delta\vec{H}^2)^2 + 7\delta(\vec{E}\cdot\vec{H})^2], \tag{2}$$

with the definitions of $\kappa = 2\alpha^2\hbar^3\epsilon_0/45m^4c^5$ and $\delta = \mu_0/\epsilon_0$. The physical constants ϵ_0 and μ_0 are known as the electric permittivity and magnetic permeability of vacuum. The first term on the right-hand side (RHS) of Eq. (2) describes the Maxwell's wave equation in vacuum and the second term is responsible for the nonlinear birefringent property of vacuum related to the four-photon interaction.

The general expressions for the electric permittivity ϵ and magnetic permeability μ can be obtained using the definitions of the electric displacement vector $\vec{D} = \overleftrightarrow{\epsilon}\vec{E}$ and magnetic field vector $\vec{B} = \overleftrightarrow{\mu}\vec{H}$:

$$D_i = \frac{\partial L}{\partial E_i} \quad \text{and} \quad B_i = -\frac{\partial L}{\partial H_i}. \tag{3}$$

Here i refers to x, y, and z. By inserting Eq. (2) into Eq. (3), the permittivity and permeability tensors for vacuum are explicitly expressed as

$$\epsilon_{ij} = \epsilon_0\delta_{ij} + \epsilon_0\kappa[2(\vec{E}^2 - \delta\vec{H}^2)\delta_{ij} + 7\delta H_i H_j] \tag{4}$$

and

$$\mu_{ij} = \mu_0\delta_{ij} + \mu_0\kappa[2(\vec{E}^2 - \delta\vec{H}^2)\delta_{ij} - 7E_i E_j]. \tag{5}$$

Here δ_{ij} is the Kronecker delta given by 1 when $i = j$ and 0 when $i \neq j$. Since $\kappa \approx 9 \times 10^{-37} \ll 1$, Eq. (4) states that an electric field strength of $\sim 10^{17}$ V/m induces a change in the permittivity by approximately 1.8%. From the perspective of a high-power laser, such an ultrastrong field strength can be achieved by 4π-spherically-focusing a CV (radially or azimuthally polarized) 100 PW or higher-power laser pulse within a FWHM focal volume of $\lambda^3/20$ [37].
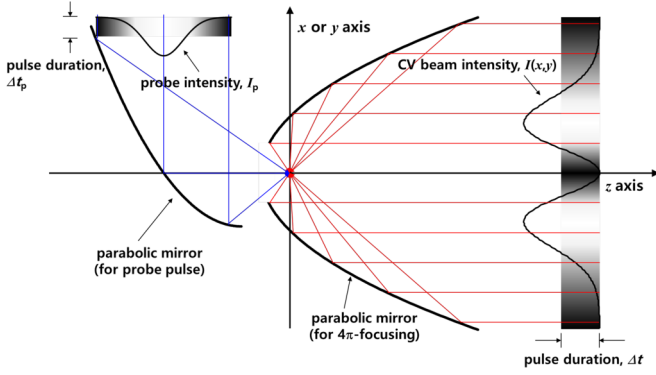
FIG. 1. Schematics for light scattering by a 4π-spherically-focused ultrastrong laser pulse. A cylindrical vector femtosecond high-power laser pulse is 4π-spherically-focused by the parabolic mirror from the right to form a nonlinear birefringent vacuum. A probe laser pulse is focused from the left and propagates through the nonlinear birefringent vacuum.

In order to have explicit forms for the permittivity and permeability tensors of the vacuum with an ultrastrong field, let us assume that a high-power CV laser pulse is spherically focused onto vacuum and another high-power probe laser pulse propagates through the vacuum region (see Fig. 1). There are two modes generated at the focus when focusing CV beams: TM mode by the radially polarized case and TE mode by the azimuthally polarized case.

A. Nonlinear birefringent vacuum induced by the transverse magnetic mode field

First, let us consider an NBV induced by the TM mode case. The electric and magnetic field distributions for the TM mode EM wave are described by [37]

$$\vec{E}_{\text{TM}} = i\hat{\theta} E_{\text{peak}} \exp[i(kr_{\text{VFS}} - \omega t)] a(r', \theta') \qquad (6a)$$

and

$$\vec{H}_{\text{TM}} = -\hat{\phi} H_{\text{peak}} \exp[i(kr_{\text{VFS}} - \omega t)] b(r', \theta'). \qquad (6b)$$

Here E_{peak} (or H_{peak}) is the peak field strength defined by $\pi k r_{\text{VFS}} E_{\text{VFS}}/2$ (or $E_{\text{peak}}/\mu_0 c$) and k is the wave number of the EM wave. The E_{VFS} is the field strength on a virtual focusing sphere (VFS) which can be directly calculated from the incident field strength or laser power. The r_{VFS} is the distance between the VFS and the focus. The constant phase factor $\exp(ikr_{\text{VFS}})$ can be dropped without loss of generality, and $a(r', \theta')$ and $b(r', \theta')$ are spatial distribution functions for the E and B fields given by

$$a(r', \theta') = j_0(kr') + \frac{5}{2^3} j_2(kr') P_2(\cos\theta')$$
$$- \frac{9}{2^6} j_4(kr') P_4(\cos\theta') + \cdots \qquad (7)$$

and

$$b(r', \theta') = \frac{4}{\pi} j_1(kr') \sin\theta'. \qquad (8)$$

Here $j_n(x)$ and $P_n(x)$ are the nth order spherical Bessel function and Legendre function, respectively. As shown in Eqs. (6)–(8), a standing wave is formed near the focus when 4π-spherically-focusing the EM wave.

Since the change in the field strength occurs over a much longer time than the Compton time, it is assumed that the field strength instantaneously changes the permittivity and permeability of vacuum. The permittivity and permeability tensors in spherical coordinates can be written by

$$\overleftrightarrow{\epsilon}_{\text{TM}} = \begin{bmatrix} \epsilon_O & 0 & 0 \\ 0 & \epsilon_O & 0 \\ 0 & 0 & \epsilon_E \end{bmatrix} \quad \text{and} \quad \overleftrightarrow{\mu}_{\text{TM}} = \begin{bmatrix} \mu_O & 0 & 0 \\ 0 & \mu_E & 0 \\ 0 & 0 & \mu_O \end{bmatrix},$$
$$(9)$$

with expressions of the E and B fields in matrix form in spherical coordinates as

$$\vec{E}_{\text{TM}} = \begin{bmatrix} 0 \\ E_{\text{TM}} \\ 0 \end{bmatrix} \quad \text{and} \quad \vec{H}_{\text{TM}} = \begin{bmatrix} 0 \\ 0 \\ H_{\text{TM}} \end{bmatrix}. \qquad (10)$$

Here $E_{\text{TM}} = E_{\text{peak}} a(r', \theta') \sin(\omega t)$ and $H_{\text{TM}} = -(E_{\text{peak}}/\mu_0 c) b(r', \theta') \cos(\omega t)$ from Eq. (6). The subscripts O and E in Eq. (9) mean the ordinary and extraordinary tensor elements, respectively. The ordinary and extraordinary elements are explicitly expressed as follows:

$$\epsilon_O = \epsilon_0 + 2\epsilon_0\kappa \left(E_{\text{TM}}^2 - \delta H_{\text{TM}}^2 \right), \qquad (11a)$$

$$\epsilon_E = \epsilon_0 + \epsilon_0\kappa \left(2E_{\text{TM}}^2 + 5\delta H_{\text{TM}}^2 \right), \qquad (11b)$$

$$\mu_O = \mu_0 + 2\mu_0\kappa \left(E_{\text{TM}}^2 - \delta H_{\text{TM}}^2 \right), \qquad (11c)$$

and

$$\mu_E = \mu_0 - \mu_0\kappa \left(5E_{\text{TM}}^2 + 2\delta H_{\text{TM}}^2 \right). \qquad (11d)$$

Therefore, from Eq. (9), a general expression of the refractive index tensor for vacuum can be obtained as

$$\overleftrightarrow{n}_{\text{TM}}^2 = \overleftrightarrow{\epsilon}_{\text{TM}} \overleftrightarrow{\mu}_{\text{TM}} = \begin{bmatrix} \epsilon_O\mu_O & 0 & 0 \\ 0 & \epsilon_O\mu_E & 0 \\ 0 & 0 & \epsilon_E\mu_O \end{bmatrix}. \qquad (12)$$

Since $\kappa\vec{E}_{\text{TM}}^2 \gg \kappa^2\vec{E}_{\text{TM}}^4$, tensor elements in Eq. (12) are approximated as

$$\epsilon_O\mu_O \approx \epsilon_0\mu_0 + 4\epsilon_0\mu_0\kappa \left(E_{\text{TM}}^2 - \delta H_{\text{TM}}^2 \right), \qquad (13a)$$

$$\epsilon_O\mu_E \approx \epsilon_0\mu_0 - \epsilon_0\mu_0\kappa \left(3E_{\text{TM}}^2 + 4\delta H_{\text{TM}}^2 \right), \qquad (13b)$$

and

$$\epsilon_E\mu_O \approx \epsilon_0\mu_0 + \epsilon_0\mu_0\kappa \left(4E_{\text{TM}}^2 + 3\delta H_{\text{TM}}^2 \right). \qquad (13c)$$

Equation (13) shows the nonlinear birefringent property of the vacuum. For the case of a pure magnetic field ($E_{\text{TM}} = 0$), one obtains $\epsilon_O\mu_O = \epsilon_O\mu_E \approx \epsilon_0\mu_0 - 4\epsilon_0\mu_0\kappa\delta H_{\text{TM}}^2$ and $\epsilon_E\mu_O \approx \epsilon_0\mu_0 + 3\epsilon_0\mu_0\kappa\delta H_{\text{TM}}^2$. This expression is the same as that for the refractive index under the purely magnetic constant field with a perpendicular polarization as shown in [51]. In this case, an EM wave passing through the $\epsilon_O\mu_O - \epsilon_E\mu_O$ or $\epsilon_O\mu_E - \epsilon_E\mu_O$ plane will experience a nonlinear birefringence due to the strong magnetic field. The ongoing PVLAS experiment [17] which uses a sensitive polarimeter based on a high finesse Fabry-Perot cavity pursues to experimentally demonstrate the vacuum magnetic birefringence and to assess dispersive QED strong field effects under a constant and strong magnetic field. For the case of a pure electric field ($H_{\text{TM}} = 0$), one obtains $\epsilon_O\mu_O = \epsilon_E\mu_O \approx \epsilon_0\mu_0 + 4\epsilon_0\mu_0\kappa E_{\text{TM}}^2$

and $\epsilon_O\mu_E \approx \epsilon_0\mu_0 - 3\epsilon_0\mu_0\kappa E_{\mathrm{TM}}^2$. An EM wave propagating in this vacuum will experience a similar nonlinear birefringent property as well. The refractive index for vacuum under an ultrastrong laser intensity can be expressed by the well-known Kerr nonlinearity as $n = 1 + n_{2,\mathrm{vac}}I$ [5]. By using the relationship of $I = c\epsilon_0 E^2/2$, the nonlinear refractive index $n_{2,\mathrm{vac}}$ is given by

$$n_{2,\mathrm{vac}} = 4\frac{\kappa}{c\epsilon_0} \quad \text{or} \quad n_{2,\mathrm{vac}} = -3\frac{\kappa}{c\epsilon_0}, \qquad (14)$$

depending on the propagation direction. The calculation shows that the nonlinear refractive index of vacuum ($n_{2,\mathrm{vac}} = 1.36 \times 10^{-29}$ cm^2/W for $n_{2,\mathrm{vac}} = 4\kappa/c\epsilon_0$) is 3×10^{10} times lower than that of air ($n_{2,\mathrm{air}} = 4 \times 10^{-19}$ cm^2/W) at 800 nm wavelength [52] and 10^{19} times lower than that of water [53].

B. Nonlinear birefringent vacuum induced by the transverse electric mode field

The NBV induced by the TE mode EM wave can be derived in the same way. In this case, the electric and magnetic fields for the TE mode EM wave are written by

$$\vec{E}_{\mathrm{TE}} = -\hat{\phi}E_{\mathrm{peak}}\exp[i(kr_{\mathrm{VFS}} - \omega t)]b(r', \theta') \qquad (15a)$$

and

$$\vec{H}_{\mathrm{TE}} = i\hat{\theta}H_{\mathrm{peak}}\exp[i(kr_{\mathrm{VFS}} - \omega t)]a(r', \theta'). \qquad (15b)$$

The E and B fields in matrix form in spherical coordinates are written as

$$\vec{E}_{\mathrm{TE}} = \begin{bmatrix} 0 \\ 0 \\ E_{\mathrm{TE}} \end{bmatrix} \quad \text{and} \quad \vec{H}_{\mathrm{TE}} = \begin{bmatrix} 0 \\ H_{\mathrm{TE}} \\ 0 \end{bmatrix}, \qquad (16)$$

with $E_{\mathrm{TE}} = -E_{\mathrm{peak}}b(r', \theta')\cos(\omega t)$ and $H_{\mathrm{TE}} = (E_{\mathrm{peak}}/\mu_0 c)a(r', \theta')\sin(\omega t)$. Then the permittivity and permeability tensors for the TE mode EM wave case is explicitly given by

$$\overleftrightarrow{\epsilon}_{\mathrm{TE}} = \begin{bmatrix} \epsilon_O & 0 & 0 \\ 0 & \epsilon_E & 0 \\ 0 & 0 & \epsilon_O \end{bmatrix} \quad \text{and} \quad \overleftrightarrow{\mu}_{\mathrm{TE}} = \begin{bmatrix} \mu_O & 0 & 0 \\ 0 & \mu_O & 0 \\ 0 & 0 & \mu_E \end{bmatrix}, \qquad (17)$$

and the general expression of the refractive index for vacuum can be obtained as

$$\overleftrightarrow{n}_{\mathrm{TE}}^2 = \overleftrightarrow{\epsilon}_{\mathrm{TE}}\overleftrightarrow{\mu}_{\mathrm{TE}} = \begin{bmatrix} \epsilon_O\mu_O & 0 & 0 \\ 0 & \epsilon_E\mu_O & 0 \\ 0 & 0 & \epsilon_O\mu_E \end{bmatrix}, \qquad (18)$$

with the definitions of the ordinary and extraordinary elements of the tensors as $\epsilon_O = \epsilon_0 + 2\epsilon_0\kappa(E_{\mathrm{TE}}^2 - \delta H_{\mathrm{TE}}^2), \epsilon_E = \epsilon_0 + \epsilon_0\kappa(2E_{\mathrm{TE}}^2 + 5\delta H_{\mathrm{TE}}^2), \quad \mu_O = \mu_0 + 2\mu_0\kappa(E_{\mathrm{TE}}^2 - \delta H_{\mathrm{TE}}^2),$ and $\mu_E = \mu_0 - \mu_0\kappa(5E_{\mathrm{TE}}^2 + 2\delta H_{\mathrm{TE}}^2)$. Again, since $\kappa\vec{E}_{\mathrm{TE}}^2 \gg \kappa^2\vec{E}_{\mathrm{TE}}^4$, tensor elements in Eq. (18) are approximated as

$$\epsilon_O\mu_O \approx \epsilon_0\mu_0 + 4\epsilon_0\mu_0\kappa(E_{\mathrm{TE}}^2 - \delta H_{\mathrm{TE}}^2), \qquad (19a)$$

$$\epsilon_E\mu_O \approx \epsilon_0\mu_0 + \epsilon_0\mu_0\kappa(4E_{\mathrm{TE}}^2 + 3\delta H_{\mathrm{TE}}^2), \qquad (19b)$$

and

$$\epsilon_O\mu_E \approx \epsilon_0\mu_0 - \epsilon_0\mu_0\kappa(3E_{\mathrm{TE}}^2 + 4\delta H_{\mathrm{TE}}^2). \qquad (19c)$$

Equations (18) and (19) also show the birefringent property of the vacuum. Finally, considering the time-dependent electric field in Eqs. (6) and (15), the tensor elements in Eqs. (12) and (18) can be expressed as

$$[\epsilon_O\mu_O]_{\mathrm{TM}} \approx \epsilon_0\mu_0 + 4\epsilon_0\mu_0\kappa\big[E_{\mathrm{peak}}^2 a^2(r', \theta')\sin^2\omega t - \delta H_{\mathrm{peak}}^2 b^2(r', \theta')\cos^2\omega t\big], \qquad (20a)$$

$$[\epsilon_O\mu_E]_{\mathrm{TM}} \approx \epsilon_0\mu_0 - \epsilon_0\mu_0\kappa\big[3E_{\mathrm{peak}}^2 a^2(r', \theta')\sin^2\omega t + 4\delta H_{\mathrm{peak}}^2 b^2(r', \theta')\cos^2\omega t\big], \qquad (20b)$$

$$[\epsilon_E\mu_O]_{\mathrm{TM}} \approx \epsilon_0\mu_0 + \epsilon_0\mu_0\kappa\big[4E_{\mathrm{peak}}^2 a^2(r', \theta')\sin^2\omega t + 3\delta H_{\mathrm{peak}}^2 b^2(r', \theta')\cos^2\omega t\big], \qquad (20c)$$

$$[\epsilon_O\mu_O]_{\mathrm{TE}} \approx \epsilon_0\mu_0 + 4\epsilon_0\mu_0\kappa\big[E_{\mathrm{peak}}^2 b^2(r', \theta')\cos^2\omega t - \delta H_{\mathrm{peak}}^2 a^2(r', \theta')\sin^2\omega t\big], \qquad (20d)$$

$$[\epsilon_E\mu_O]_{\mathrm{TE}} \approx \epsilon_0\mu_0 + \epsilon_0\mu_0\kappa\big[4E_{\mathrm{peak}}^2 b^2(r', \theta')\cos^2\omega t + 3\delta H_{\mathrm{peak}}^2 a^2(r', \theta')\sin^2\omega t\big], \qquad (20e)$$

and

$$[\epsilon_O\mu_E]_{\mathrm{TE}} \approx \epsilon_0\mu_0 - \epsilon_0\mu_0\kappa\big[3E_{\mathrm{peak}}^2 b^2(r', \theta')\cos^2\omega t + 4\delta H_{\mathrm{peak}}^2 a^2(r', \theta')\sin^2\omega t\big]. \qquad (20f)$$

Equation (20) clearly shows how the refractive index of vacuum can be a function of space-time-dependent ultrastrong electromagnetic fields.

III. SCATTERED ELECTROMAGNETIC WAVE BY AN ULTRASTRONG ELECTROMAGNETIC FIELD

A. Probe electromagnetic wave propagating NBV

In order to calculate an electric field scattered from an NBV, let us consider the E field of a probe laser pulse $\vec{E}_p$ passing through the vacuum expressed by Eqs. (12), (18), and (20). The time-dependent Maxwell's equations for the E and B fields of the probe laser pulse are written as

$$\nabla \times \vec{B} = \mu\vec{J} + \overleftrightarrow{\epsilon}\overleftrightarrow{\mu}\frac{\partial\vec{E}}{\partial t} \quad \text{and} \quad \nabla \times \vec{E} = -\frac{\partial\vec{B}}{\partial t}. \qquad (21)$$

By assuming no source for the electric charge and current and applying the curl to the electric field in Eq. (21), one obtains the following wave equation:

$$\nabla^2\vec{E} \approx \overleftrightarrow{\epsilon}\overleftrightarrow{\mu}\frac{\partial^2}{\partial t^2}\vec{E}. \qquad (22)$$

Let us assume that the probe pulse is x polarized, the pulse duration is Δt_p, and the time delay between the probe pulse and the 4π-spherically-focused laser pulse is t_d. Then, the electric field for the probe pulse can be expressed by

$$\vec{E}_p = \hat{x}E_{p0}e^{-\frac{(t-t_d)^2}{2(\Delta t_p)^2}}e^{i(k_p z - \omega_\gamma t + \delta_p)}. \qquad (23)$$

Here δ_p is the relative phase shift between the probe pulse and the 4π-spherically-focused laser pulse, and ω_γ is the angular

frequency of the probe pulse given by $k_p c$ (k_p wave number). Since $\omega_\gamma \gg 1/\Delta t$ for the typical fs high-power laser pulse, the second time derivative in Eq. (22) can be approximated as

$$\frac{\partial^2}{\partial t^2}\vec{E}_p \approx -\hat{x}\omega_\gamma^2 E_{p0} e^{-\frac{(t-t_d)^2}{2(\Delta t_p)^2}} e^{i(k_p z - \omega_\gamma t + \delta_p)}. \tag{24}$$

By inserting Eq. (24) into Eq. (22), the wave equation for the probe pulse propagating through the NBV induced by an ultrastrong laser field becomes

$$\nabla^2 \vec{E}_p + \omega_\gamma^2 \overleftrightarrow{\epsilon}\overleftrightarrow{\mu}\vec{E}_p = 0. \tag{25}$$

Since the refractive index tensor $\overleftrightarrow{\epsilon}\overleftrightarrow{\mu}$ is expressed in spherical coordinates, it is convenient to express this tensor in the Cartesian coordinate system. The tensor transformation from the spherical coordinate system to the Cartesian coordinate system can be obtained using the relationship of

$$[\overleftrightarrow{\epsilon}\overleftrightarrow{\mu}]_{\text{Cart}} = Q[\overleftrightarrow{\epsilon}\overleftrightarrow{\mu}]_{\text{sph}}Q^T, \tag{26}$$

with

$$Q = \begin{bmatrix} \sin\theta\cos\phi & \cos\theta\cos\phi & -\sin\phi \\ \sin\theta\sin\phi & \cos\theta\sin\phi & \cos\phi \\ \cos\theta & -\sin\theta & 0 \end{bmatrix}$$

and

$$Q^T = \begin{bmatrix} \sin\theta\cos\phi & \sin\theta\sin\phi & \cos\theta \\ \cos\theta\cos\phi & \cos\theta\sin\phi & -\sin\theta \\ -\sin\phi & \cos\phi & 0 \end{bmatrix}.$$

Here the angles θ and ϕ are the polar and azimuthal angles in spherical coordinates, respectively. After the transformation, the refractive index tensor in the Cartesian coordinate system $[\overleftrightarrow{\epsilon}\overleftrightarrow{\mu}]_{\text{Cart}}$ is written as

$$[\overleftrightarrow{\epsilon}\overleftrightarrow{\mu}]_{\text{Cart}} = \begin{bmatrix} \epsilon\mu_{xx} & \epsilon\mu_{xy} & \epsilon\mu_{xz} \\ \epsilon\mu_{yx} & \epsilon\mu_{yy} & \epsilon\mu_{yz} \\ \epsilon\mu_{zx} & \epsilon\mu_{zy} & \epsilon\mu_{zz} \end{bmatrix}, \tag{27}$$

with all tensor elements given by

$$\begin{aligned} \epsilon\mu_{xx} &= \epsilon_0\mu_0 + 4\epsilon_0\mu_0\kappa E_{\text{peak}}^2 \\ &\quad \times [a^2(r',\theta')\sin^2\omega t - b^2(r',\theta')\cos^2\omega t] \\ &\quad - 7\epsilon_0\mu_0\kappa E_{\text{peak}}^2[a^2(r',\theta')\cos^2\theta\cos^2\phi\sin^2\omega t \\ &\quad - b^2(r',\theta')\sin^2\phi\cos^2\omega t], \end{aligned} \tag{28a}$$

$$\begin{aligned} \epsilon\mu_{xy} = \epsilon\mu_{yx} &= -7\epsilon_0\mu_0\kappa E_{\text{peak}}^2[a^2(r',\theta')\cos^2\theta\sin^2\omega t \\ &\quad + b^2(r',\theta')\cos^2\omega t]\sin\phi\cos\phi, \end{aligned} \tag{28b}$$

$$\begin{aligned} \epsilon\mu_{xz} = \epsilon\mu_{zx} &= 7\epsilon_0\mu_0\kappa E_{\text{peak}}^2 \\ &\quad \times a^2(r',\theta')\sin\phi\cos\phi\sin^2\omega t, \end{aligned} \tag{28c}$$

$$\begin{aligned} \epsilon\mu_{yy} &= \epsilon_0\mu_0 + 4\epsilon_0\mu_0\kappa E_{\text{peak}}^2 \\ &\quad \times [a^2(r',\theta')\sin^2\omega t - b^2(r',\theta')\cos^2\omega t] \\ &\quad - 7\epsilon_0\mu_0\kappa E_{\text{peak}}^2[a^2(r',\theta')\cos^2\theta\sin^2\phi\sin^2\omega t \\ &\quad - b^2(r',\theta')\cos^2\phi\cos^2\omega t], \end{aligned} \tag{28d}$$

$$\begin{aligned} \epsilon\mu_{yz} = \epsilon\mu_{zy} &= 7\epsilon_0\mu_0\kappa E_{\text{peak}}^2 \\ &\quad \times a^2(r',\theta')\sin\theta\cos\theta\sin\phi\sin^2\omega t, \end{aligned} \tag{28e}$$

and

$$\begin{aligned} \epsilon\mu_{zz} &= \epsilon_0\mu_0 + 4\epsilon_0\mu_0\kappa E_{\text{peak}}^2 \\ &\quad \times [a^2(r',\theta')\sin^2\omega t - b^2(r',\theta')\cos^2\omega t] \\ &\quad - 7\epsilon_0\mu_0\kappa E_{\text{peak}}^2 a^2(r',\theta')\sin^2\theta\sin^2\omega t. \end{aligned} \tag{28f}$$

In the above equations, the relationship of $E_{\text{peak}}^2 = \delta H_{\text{peak}}^2$ is used.

Now, Eq. (25) is rewritten as

$$\nabla^2\vec{E}_p + \omega_\gamma^2\epsilon_0\mu_0\delta_{ij}\vec{E}_p = -\omega_\gamma^2(\overleftrightarrow{\epsilon}\overleftrightarrow{\mu} - \epsilon_0\mu_0\delta_{ij})\vec{E}_p \tag{29}$$

by separating the product of constant permittivity and permeability from the refractive index tensor. Here δ_{ij} is the Kronecker delta and i refers to x, y, and z again. By applying the Born approximation, the general solution of Eq. (29) is given by

$$\vec{E}_p = \vec{E}_{\text{inc}} + \vec{E}_S, \tag{30}$$

where $\vec{E}_{\text{inc}}$ and $\vec{E}_S$ mean the incident and scattered waves, respectively. The incident wave satisfies the wave equation $\nabla^2\vec{E}_{\text{inc}} + \omega_\gamma^2\epsilon_0\mu_0\delta_{ij}\vec{E}_{\text{inc}} = 0$ and is assumed to simply propagate in the vacuum without scattering. The incident wave is considered as the incoming probe laser pulse $\vec{E}_p$. The $\vec{E}_S$ describes the electric field scattered from the NBV and can be calculated with the Green's function as

$$\vec{E}_S = -\omega_\gamma^2 \int G(\vec{r} - \vec{r}')(\overleftrightarrow{\epsilon}\overleftrightarrow{\mu} - \epsilon_0\mu_0\delta_{ij})\vec{E}_p e^{i\vec{k}_p\cdot\vec{r}'}d^3r'. \tag{31}$$

Considering the polarization of the probe pulse ($\vec{E}_p = E_p\hat{x}$) and its propagation along the z axis near the vicinity of focus, the scattered waves for the x- and y-polarization components can be written as

$$\begin{bmatrix} E_{Sx} \\ E_{Sy} \end{bmatrix} = E_p \int G(\vec{r} - \vec{r}') \begin{bmatrix} V_x(\vec{r}') \\ V_y(\vec{r}') \end{bmatrix} e^{i\vec{k}_p\cdot\vec{r}'}d^3r', \tag{32}$$

with the explicit expressions of the scattering potential functions as

$$\begin{aligned} V_x&(r',\theta',\phi';t) \\ &= -\omega_\gamma^2(\epsilon\mu_{xx} - \epsilon_0\mu_0) \\ &= -4\kappa k_p^2 E_{\text{peak}}^2[a^2(r',\theta')\sin^2\omega t - b^2(r',\theta')\cos^2\omega t] \\ &\quad + 7\kappa k_p^2 E_{\text{peak}}^2[a^2(r',\theta')\cos^2\theta\cos^2\phi\sin^2\omega t \\ &\quad - b^2(r',\theta')\sin^2\phi\cos^2\omega t] \end{aligned} \tag{33a}$$

and

$$\begin{aligned} V_y(r',\theta',\phi';t) &= -\omega_\gamma^2\epsilon\mu_{yx} \\ &= 7\kappa k_p^2 E_{\text{peak}}^2[a^2(r',\theta')\cos^2\theta\sin^2\omega t \\ &\quad + b^2(r',\theta')\cos^2\omega t]\sin\phi\cos\phi. \end{aligned} \tag{33b}$$

The phenomenon of multiple scattering is not considered due to the weak light-light scattering characteristics. Then, the first-order solution for the scattered probe pulse can be

written as

$$E_{Sx,Sy}(r;t)$$

$$= -E_{p0}e^{-\frac{(t-t_d)^2}{2(\Delta t_p)^2}}\frac{e^{i(k_p z-\omega_\gamma t+\delta_p)}}{4\pi r}\int e^{-i\vec{q}\cdot\vec{r}'}V_{x,y}(\vec{r}';t)d^3r'. \quad (34)$$

Here the vector $\vec{q}$, known as the scattering vector, is defined by $\vec{k}-\vec{k}_0$, which describes the momentum transfer from the focused ultrastrong laser pulse to the probe pulse. Since the elastic scattering of the probe pulse is considered, the

magnitude of the scattering vector q is given by $2k_p\sin(\theta/2)$ (see Fig. 2). In the following sections the first-order solution for the specific scattering potential function given by the 4π-spherically-focused light field is presented.

B. Electromagnetic field scattered by the nonlinear birefringent vacuum

Let us first calculate the x-polarized scattered E field. Hereafter, this is referred to as the x-pol/x-pol scattering case. By putting Eq. (33a) into Eq. (34), the x-polarized scattered E field E_{Sx} is explicitly expressed as

$$E_{Sx} = 4\kappa k_p^2 E_{\text{peak}}^2 E_{p0}e^{-\frac{(t-t_d)^2}{2\Delta t_p^2}}\frac{e^{i(k_p z-\omega_\gamma t+\delta_p)}}{4\pi r}\int d^3r' e^{-i\vec{q}\cdot\vec{r}'}[a^2(r',\theta')\sin^2\omega t - b^2(r',\theta')\cos^2\omega t]$$

$$- 7\kappa k_p^2 E_{\text{peak}}^2 E_{p0}e^{-\frac{(t-t_d)^2}{2\Delta t_p^2}}\frac{e^{i(k_p z-\omega_\gamma t+\delta_p)}}{4\pi r}\int d^3r' e^{-i\vec{q}\cdot\vec{r}'}[a^2(r',\theta')\cos^2\theta\cos^2\phi\sin^2\omega t - b^2(r',\theta')\sin^2\phi\cos^2\omega t]. \quad (35)$$

Equation (35) consists of two integrals: $I_1 = \int e^{-i\vec{q}\cdot\vec{r}'}a^2(r',\theta')d^3r'$ (contribution by the E field) and $I_2 = \int e^{-i\vec{q}\cdot\vec{r}'}b^2(r',\theta')d^3r'$ (contribution by the H field). For convenience, $(\Delta t_p)^2$ is replaced by Δt_p^2. The phase term $e^{-i\vec{q}\cdot\vec{r}'}$ in Eq. (35) is expanded by using the plane wave expansion, in terms of spherical Bessel functions $j_l(x)$ and associated Legendre polynomials $P_l^m(x)$ as follows:

$$\exp\left(-iqr'\cos\gamma\right) = \sum_{l=0}^{\infty}(2l+1)(-i)^l j_l(qr')\sum_{v=-l}^{l}\frac{\Gamma(l-v+1)}{\Gamma(l+v+1)}P_l^v(\cos\zeta)P_l^v(\cos\theta')\exp[iv(\phi-\phi')]. \quad (36)$$

The angle γ between the $\vec{q}$ and $\vec{r}'$ vectors is given by $\zeta-\theta'$ with $\zeta = (\pi+\theta)/2$ [see Fig. 2(b)]. The field distribution term $a^2(r',\theta')$ in I_1 can be expressed as

$$a^2(r',\theta') = \sum_{n=0}^{2}\sum_{m=0}^{2}\left[\alpha_{nm}\frac{4n+1}{2^{3n}}\frac{4m+1}{2^{3m}}j_{2n}(kr')j_{2m}(kr')\right.$$

$$\left.\times P_{2n}(\cos\theta')P_{2m}(\cos\theta')\right] + HO, \quad (37)$$

where HO means the higher-order terms. The coefficient α_{nm} is given by 1 when $n=m$, and 2 when $n\neq m$. The expression $\frac{4n+1}{2^{3n}}\frac{4m+1}{2^{3m}}$ is valid only when n and m are less than 2. The exact expression for the higher-order terms can be found in [37]. Similarly, the field distribution term $b^2(r',\theta')$ in I_2 can be expressed as

$$b^2(r',\theta') = \frac{4^2}{\pi^2}j_1^2(kr')\sin^2\theta'. \quad (38)$$

Since the contribution by higher-order terms is negligible, the lowest-order term ($l=n=m=0$) will be taken into account in the calculation. This consideration simplifies integrals I_1 and I_2 as

$$I_1 = \int e^{-i\vec{q}\cdot\vec{r}'}a^2(r',\theta')d^3r' = 4\pi\int dr'\, j_0(qr')j_0^2(kr')r'^2 \quad (39a)$$

and

$$I_2 = \int e^{-i\vec{q}\cdot\vec{r}'}b^2(r',\theta')d^3r'$$

$$= \frac{8\pi}{3}\left(\frac{4^2}{\pi^2}\right)\int dr'\, j_0(qr')j_1^2(kr')r'^2. \quad (39b)$$
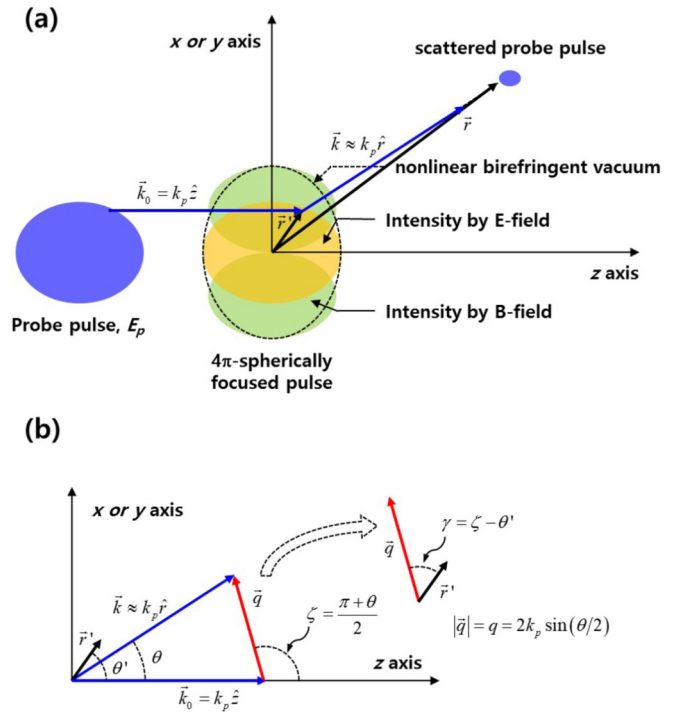

FIG. 2. (a) The probe laser pulse is scattered from the nonlinear birefringent vacuum induced by the 4π-spherical-focused femtosecond high-power laser pulse. (b) The probe laser pulse initially propagates through the z axis and the scattered probe pulse is scattered with a propagation vector $\vec{k}$. The magnitude of the scattering vector $\vec{q} = \vec{k} - \vec{k}_0$ is given by $2k_p\sin(\theta/2)$ when the scattered probe pulse is elastic.

The integrals of the product of the three spherical Bessel functions are given by

$$\int_0^\infty j_0(qr') j_0^2(kr') r'^2 dr' = \frac{\pi}{4k^2 q} \quad (40a)$$

and

$$\int_0^\infty j_0(qr') j_1^2(kr') r'^2 dr' = \frac{\pi}{4k^2 q} P_1(\cos\theta), \quad (40b)$$

with the help of the following integral identity [54]:

$$\int_0^\infty r^{1-\mu} J_\mu(qr) J_\nu(kr) J_\nu(kr) dr$$
$$= \frac{1}{\sqrt{2\pi}} q^{-\mu} (k^2)^{\mu-1} (\sin a)^{\mu-\frac{1}{2}} P_{\nu-\frac{1}{2}}^{\frac{1}{2}-\mu}(\cos a), \quad (41)$$

with the definition of $\cos a = (2k^2 - q^2)/2k^2$. After summarizing the above results, the following result is obtained for the x-polarized scattered E field:

$$E_{Sx} = \pi \kappa E_{\text{peak}}^2 E_{p0} e^{-\frac{(t-t_d)^2}{2\Delta t_p^2}} \frac{e^{i(k_p z - \omega_\gamma t + \delta_p)}}{r} \frac{1}{q}$$
$$\times \left[\sin^2 \omega t - \frac{2}{3}\left(\frac{4}{\pi}\right)^2 P_1(\cos\theta)\cos^2 \omega t \right]$$
$$- \frac{7\pi}{4} \kappa E_{\text{peak}}^2 E_{p0} e^{-\frac{(t-t_d)^2}{2\Delta t_p^2}} \frac{e^{i(k_p z - \omega_\gamma t + \delta_p)}}{r} \frac{1}{q}$$
$$\times \left[\cos^2\theta \cos^2\phi \sin^2 \omega t \right.$$
$$\left. - \frac{2}{3}\left(\frac{4}{\pi}\right)^2 P_1(\cos\theta)\sin^2\phi \cos^2 \omega t \right]. \quad (42)$$

The difference in coefficients [1 and $(2/3)\cdot(4/\pi)^2$] between the first and the second terms in the parentheses is 8%, originating from taking only the lowest-order term during the integral calculation of Eq. (39a). Considering that the electric field energy should be the same as the magnetic field energy, Eq. (42) should be rewritten as

$$E_{Sx} = f_{xx}(\theta, \phi, t) E_{p0} e^{-\frac{(t-t_d)^2}{2\Delta t_p^2}} \frac{e^{i(k_p z - \omega_\gamma t + \delta_p)}}{r}, \quad (43)$$

with the definition of the scattering amplitude $f_{xx}(\theta, \phi, t)$ for the NBV as

$$f_{xx}(\theta, \phi, t)$$
$$= \frac{8\kappa E_{\text{peak}}^2}{3\pi q}[4(\sin^2 \omega t - \cos\theta \cos^2 \omega t)$$
$$- 7\cos\theta(\cos\theta \cos^2\phi \sin^2 \omega t - \sin^2\phi \cos^2 \omega t)]. \quad (44)$$

By inserting Eq. (33b) into Eq. (34), the scattered E field for the y polarization (hereafter x-pol/y-pol scattering case) E_{Sy} is given by

$$E_{Sy} = -7\kappa E_{\text{peak}}^2 E_{p0} e^{-\frac{(t-t_d)^2}{2\Delta t_p^2}} \frac{e^{i(k_p z - \omega_\gamma t + \delta_p)}}{4\pi r} \int d^3 r' e^{-i\vec{q}\cdot\vec{r}'}$$
$$\times [a^2(r', \theta')\cos^2\theta \sin^2 \omega t + b^2(r', \theta')\cos^2 \omega t]. \quad (45)$$

Again, by taking similar mathematical steps with the integrals of I_1 and I_2, one obtains the scattered E field for y polarization E_{Sy} as

$$E_{Sy} = f_{xy}(\theta, \phi, t) E_{p0} e^{-\frac{(t-t_d)^2}{2\Delta t_p^2}} \frac{e^{i(k_p z - \omega_\gamma t + \delta_p)}}{r}, \quad (46)$$

with a different definition of the scattering amplitude $f_{xy}(\theta, \phi, t)$ for the NBV as

$$f_{xy}(\theta, \phi, t) = \frac{8\kappa E_{\text{peak}}^2}{3\pi q} 7(\cos^2\theta \sin^2 \omega t$$
$$+ \cos\theta \cos^2 \omega t)\sin\phi\cos\phi. \quad (47)$$

The peak field strength E_{peak} can be calculated from the laser power P_L as $(k/4)\sqrt{3\pi P_L/c\epsilon_0}$. Equations (43) and (46) show the instantaneously scattered E field at a certain scattering angle of θ and ϕ. This expression provides information on the angular distribution of the electric fields scattered from a spherically-focused ultrastrong laser pulse. For comparison, other expressions for photons scattered under static field conditions can be found in [55,56]. By replacing κ by $\alpha/90\pi E_{\text{Sch}}^2$ with the Schwinger field of $E_{\text{Sch}} = m_e^2 c^3/e\hbar$ and the fine structure constant of $\alpha = e^2/4\pi\epsilon_0\hbar c \approx 1/137$, the scattering amplitudes for the x-pol/x-pol and x-pol/y-pol scattering cases convert to

$$f_{xx}(\theta, \phi, t)$$
$$= \frac{4\alpha}{135\pi^2}\left(\frac{E_{peak}}{E_{Sch}}\right)^2 \frac{1}{q}[4(\sin^2 \omega t - \cos\theta \cos^2 \omega t)$$
$$- 7\cos\theta(\cos\theta \cos^2\phi \sin^2 \omega t - \sin^2\phi \cos^2 \omega t)] \quad (48)$$

and

$$f_{xy}(\theta, \phi, t) = \frac{4\alpha}{135\pi^2}\left(\frac{E_{\text{peak}}}{E_{\text{Sch}}}\right)^2 \frac{1}{q} 7(\cos^2\theta \sin^2 \omega t$$
$$+ \cos\theta \cos^2 \omega t)\sin\phi\cos\phi. \quad (49)$$

C. Estimation of the number of scattered photons

Since the scattering amplitude is proportional to $(E_{\text{peak}}/E_{\text{Sch}})^2$, the scattered probe pulse by the NBV is in general too weak to be detected. Therefore, it is convenient to calculate the number of photons scattered from the NBV. In order to calculate the number of scattered photons, let us first calculate the scattered EM energy. The energy of the scattered probe pulse $\mathcal{E}_S$ is calculated by taking the volume integral of Eqs. (43) and (46) as

$$\mathcal{E}_S = \frac{1}{2}c\epsilon_0 \int E_S^2 r^2 dr d\Omega, \quad (50)$$

where $d\Omega$ is the infinitesimal solid angle defined as $\sin\theta d\theta d\phi$. Using the relationship of $\mathcal{E}_S = N_S \hbar\omega_\gamma$, the number of scattered photons per solid angle $\frac{dN_S}{d\Omega}$ is given by

$$\frac{dN_S}{d\Omega} = \frac{\epsilon_0 E_{p0}^2}{2\hbar\omega_\gamma} \int dr \frac{d\sigma}{d\Omega} e^{-\frac{(t-t_d)^2}{\Delta t_p^2}} \cos^2(\omega_\gamma t - \delta_p), \quad (51)$$

with the definition of the differential cross section as $d\sigma(\theta, \phi, t)/d\Omega = |f(\theta, \phi, t)|^2$. In Eq. (51), the integration in the r direction can be regarded as the integration in time,

i.e., $dr = cdt$. The probe laser pulse is assumed to be focused within a radius of λ_p for an efficient scattering event. With a flat-top uniform beam profile, the radius w_p is given by the first minimum value of the Airy function as $1.22 \times f\lambda_p/D$. Here f is the focal length of a focusing optic and D is the beam diameter, respectively. This radius of λ_p can be achieved with a focusing condition of f number (f/D) of $\sim$0.82. The total number of incident photons of the probe laser pulse can be estimated from

$$N_p = \frac{c\epsilon_0 E_{p0}^2}{2\hbar\omega_\gamma} \int_0^\infty dt\, e^{-\frac{(t-t_d)^2}{\Delta t_p^2}} 2\pi \int_0^\infty \rho d\rho e^{-\frac{\rho^2}{\lambda_p^2}}. \quad (52)$$

Thus, the relation between the photon number and the field strength is obtained as

$$E_{p0}^2 \approx \frac{4N_p \hbar\omega_\gamma}{\sqrt{\pi}\epsilon_0 c \Delta t_p \pi \lambda_p^2}. \quad (53)$$

After inserting Eq. (53) into Eq. (51) and converting the integral in the r direction into the integral in time, the number of scattered photons per solid angle is expressed as

$$\frac{dN_S}{d\Omega} = \frac{2N_p}{\sqrt{\pi}\Delta t_p \pi \lambda_p^2} \int dt \frac{d\sigma}{d\Omega} e^{-\frac{(t-t_d)^2}{\Delta t_p^2}} \cos^2(\omega_\gamma t - \delta_p). \quad (54)$$

Now, let us calculate the number of photons scattered from the 4π-spherically-focused ultra-strong laser pulse with a pulse duration of Δt. Two cases, such as x-pol/x-pol and x-pol/y-pol scatterings, are considered in the following calculations. For the x-pol/x-pol scattering case, the differential cross section is expressed as

$$\frac{d\sigma_{xx}(\theta, \phi, t)}{d\Omega}$$
$$= \frac{C^2}{q^2} e^{-\frac{2t^2}{\Delta t^2}} [4(\sin^2 \omega t - \cos\theta \cos^2 \omega t)$$
$$- 7\cos\theta(\cos\theta \cos^2\phi \sin^2\omega t - \sin^2\phi \cos^2\omega t)]^2, \quad (55)$$

where $(4\alpha/135\pi^2)(E_{\text{peak}}/E_{\text{Sch}})^2$ is replaced by C in Eq. (55). Considering Eqs. (54) and (55), it is evident that the strongest scattered E field is obtained with no time delay between the probe pulse and the focused pulse, i.e., $t_d = 0$. After some straightforward mathematical steps, Eq. (54) can be presented in the form of

$$\frac{dN_{S,xx}}{d\Omega} = \frac{2N_p}{\sqrt{\pi}\Delta t_p \pi \lambda_p^2} \frac{C^2}{q^2} [(4 - 7\cos^2\theta \cos^2\phi)^2 I_{\sin}$$
$$+ \cos^2\theta(4 - 7\sin^2\phi)^2 I_{\cos} - 2\cos\theta$$
$$\times (4 - 7\cos^2\theta \cos^2\phi)(4 - 7\sin^2\phi)I_{\sin\cos}]. \quad (56)$$

Here the integrals $I_{\sin}$, $I_{\cos}$, and $I_{\sin\cos}$ are defined as follows:

$$I_{\sin} = \int_0^\infty dt\, e^{-\frac{2t^2}{\Delta t^2} - \frac{t^2}{\Delta t_p^2}} \sin^4 \omega t \cos^2(\omega_\gamma t - \delta_p), \quad (57a)$$

$$I_{\cos} = \int_0^\infty dt\, e^{-\frac{2t^2}{\Delta t^2} - \frac{t^2}{\Delta t_p^2}} \cos^4 \omega t \cos^2(\omega_\gamma t - \delta_p), \quad (57b)$$

and

$$I_{\sin\cos} = \int_0^\infty dt\, e^{-\frac{2t^2}{\Delta t^2} - \frac{t^2}{\Delta t_p^2}} \sin^2 \omega t \cos^2 \omega t \cos^2(\omega_\gamma t - \delta_p). \quad (57c)$$

Reducing the power of trigonometric functions in Eq. (57) generates the sin and cos terms containing ω_γ, $\omega \pm \omega_\gamma$, and $2\omega \pm \omega_\gamma$, and those integrals can be analytically calculated using the integral identities of [54]

$$\int_0^\infty dt\, e^{-at^2} \cos\omega t\, dt = \frac{1}{2}\sqrt{\frac{\pi}{a}} \exp\left(-\frac{\omega^2}{4a}\right) \quad (58a)$$

and

$$\int_0^\infty dt\, e^{-at^2} \sin\omega t\, dt = \frac{\omega}{2a} \exp\left(-\frac{\omega^2}{4a}\right) {}_1F_1\left(\frac{1}{2}; \frac{3}{2}; \frac{\omega^2}{4a}\right). \quad (58b)$$

Here ${}_1F_1(\cdot)$ is the confluent hypergeometric (CH) function of the first kind. Due to the properties of the exponent function and of the product of the exponent on the confluent hypergeometric function, the terms containing $\omega_- = \omega - \omega_\gamma$ or $\omega_{2-} = 2\omega - \omega_\gamma$ become more dominant than the $\omega_+ = \omega + \omega_\gamma$ and $\omega_{2+} = 2\omega + \omega_\gamma$ terms. Thus, the final results of Eq. (57) can be approximated as

$$I_{\sin} \approx \frac{\sqrt{\pi}}{32} \frac{\Delta t_p}{\sqrt{1 + 2(\Delta t_p^2/\Delta t^2)}}$$
$$\times \left[3 - 2\cos 2\delta_p \exp\left(-\frac{\omega_-^2 \Delta t_p^2}{1 + 2(\Delta t_p^2/\Delta t^2)}\right) \right.$$
$$\left. + \frac{1}{2}\cos 2\delta_p \exp\left(-\frac{2\omega_{2-}^2 \Delta t_p^2}{1 + 2(\Delta t_p^2/\Delta t^2)}\right) \right], \quad (59a)$$

$$I_{\cos} \approx \frac{\sqrt{\pi}}{32} \frac{\Delta t_p}{\sqrt{1 + 2(\Delta t_p^2/\Delta t^2)}}$$
$$\times \left[3 + 2\cos 2\delta_p \exp\left(-\frac{\omega_-^2 \Delta t_p^2}{1 + 2(\Delta t_p^2/\Delta t^2)}\right) \right.$$
$$\left. + \frac{1}{2}\cos 2\delta_p \exp\left(-\frac{2\omega_{2-}^2 \Delta t_p^2}{1 + 2(\Delta t_p^2/\Delta t^2)}\right) \right], \quad (59b)$$

and

$$I_{\sin\cos} \approx \frac{\sqrt{\pi}}{32} \frac{\Delta t_p}{\sqrt{1 + 2(\Delta t_p^2/\Delta t^2)}}$$
$$\times \left[1 - \frac{1}{2}\cos 2\delta_p \exp\left(-\frac{2\omega_{2-}^2 \Delta t_p^2}{1 + 2(\Delta t_p^2/\Delta t^2)}\right) \right]. \quad (59c)$$

The exponential terms in Eq. (59) can be ignored when $\omega_-, \omega_{2-} \neq 0$. In this case, the integrals become

$$I_{\sin} = I_{\cos} \approx \frac{3\sqrt{\pi}}{32} \frac{\Delta t_p}{\sqrt{1 + 2(\Delta t_p^2/\Delta t^2)}} \quad (60a)$$

and

$$I_{\sin\cos} \approx \frac{\sqrt{\pi}}{32} \frac{\Delta t_p}{\sqrt{1 + 2\left(\Delta t_p^2/\Delta t^2\right)}}, \tag{60b}$$

and for the x-pol/x-pol scattering case the number of scattered photons per solid angle is given by

$$\frac{dN_{S,xx}}{d\Omega} = \frac{N_p}{2^4 \cdot 135^2 \cdot \pi^7} \frac{\alpha^2 (I_{\text{peak}}/I_{\text{Sch}})^2}{\sqrt{1 + 2\left(\Delta t_p^2/\Delta t^2\right)}} \Theta_{xx}(\theta, \phi), \tag{61}$$

with the definition of the angular distribution function $\Theta_{xx}(\theta, \phi)$ as

$$\begin{aligned}\Theta_{xx}(\theta, \phi) = &\frac{1}{\sin^2(\theta/2)} \{[4(1 - \cos\theta) \\ &- 7\cos\theta(\cos\theta\cos^2\phi - \sin^2\phi)]^2 \\ &+ 2[(4 - 7\cos^2\theta\cos^2\phi)^2 \\ &+ \cos^2\theta(4 - 7\sin^2\phi)^2]\}.\end{aligned} \tag{62}$$

When $\omega_- = 0$, the integrals in Eq. (59) are approximated as

$$I_{\sin} \approx \frac{\sqrt{\pi}}{32} \frac{\Delta t_p}{\sqrt{1 + 2\left(\Delta t_p^2/\Delta t^2\right)}} (3 - 2\cos 2\delta_p), \tag{63a}$$

$$I_{\cos} \approx \frac{\sqrt{\pi}}{32} \frac{\Delta t_p}{\sqrt{1 + 2\left(\Delta t_p^2/\Delta t^2\right)}} (3 + 2\cos 2\delta_p), \tag{63b}$$

and

$$I_{\sin\cos} \approx \frac{\sqrt{\pi}}{32} \frac{\Delta t_p}{\sqrt{1 + 2\left(\Delta t_p^2/\Delta t^2\right)}}, \tag{63c}$$

and the scattering event starts to experience the effect of phase delay δ_p. In this case, the angular distribution function $\Theta_{xx}^{\omega-}(\theta, \phi)$ is given as a function of phase delay by

$$\begin{aligned}\Theta_{xx}^{\omega-}(\theta, \phi, \delta_p) = &\frac{1}{\sin^2(\theta/2)} \{[4(1 - \cos\theta) \\ &- 7\cos\theta(\cos\theta\cos^2\phi - \sin^2\phi)]^2 \\ &+ 4\sin^2\delta_p(4 - 7\cos^2\theta\cos^2\phi)^2 \\ &+ 4\cos^2\delta_p\cos^2\theta(4 - 7\sin^2\phi)^2\}.\end{aligned} \tag{64}$$

Similarly, the angular distribution function for the case of $\omega_{2-} = 0$ is given by

$$\begin{aligned}\Theta_{xx}^{2\omega-}(\theta, \phi, \delta_p) = &\frac{1}{\sin^2(\theta/2)} \Big\{\frac{5}{2}[4(1 - \cos\theta) \\ &- 7\cos\theta(\cos\theta\cos^2\phi - \sin^2\phi)]^2 \\ &+ 2\cos\theta(4 - 7\cos^2\theta\cos^2\phi)(4 - 7\sin^2\phi) \\ &+ \cos^2\delta_p[(4 - 7\cos^2\theta\cos^2\phi) \\ &+ \cos^2\theta(4 - 7\sin^2\phi)]^2\Big\}.\end{aligned} \tag{65}$$

Next, let us calculate the number of scattered photons per solid angle for the x-pol/y-pol scattering case. Following similar mathematical procedures with Eqs. (49) and (54), the number of scattered photons per solid angle is explicitly given by

$$\frac{dN_{S,xy}}{d\Omega} = \frac{N_p}{2^4 \cdot 135^2 \cdot \pi^7} \frac{\alpha^2 (I_{\text{peak}}/I_{\text{Sch}})^2}{\sqrt{1 + 2\left(\Delta t_p^2/\Delta t^2\right)}} \Theta_{xy}(\theta, \phi), \tag{66}$$

where the angular distribution function is defined as

$$\Theta_{xy}(\theta, \phi) = \frac{\cos^2\theta\sin^2\phi\cos^2\phi}{\sin^2(\theta/2)} 7^2(3\cos^2\theta + 2\cos\theta + 3) \quad (\text{for} \ \omega_-, \omega_{2-} \neq 0), \tag{67a}$$

$$\Theta_{xy}^{\omega-}(\theta, \phi, \delta_p) = \frac{\cos^2\theta\sin^2\phi\cos^2\phi}{\sin^2(\theta/2)} 7^2(3\cos^2\theta + 2\cos\theta + 3 + 2\cos 2\delta_p\sin^2\theta) \quad (\text{for} \ \omega_- = 0), \tag{67b}$$

and

$$\Theta_{xy}^{2\omega-}(\theta, \phi, \delta_p) = \frac{\cos^2\theta\sin^2\phi\cos^2\phi}{\sin^2(\theta/2)} 7^2\left(3\cos^2\theta + 2\cos\theta + 3 + 2\cos 2\delta_p\sin^4\frac{\theta}{2}\right) \quad (\text{for} \ \omega_{2-} = 0). \tag{67c}$$

The expressions of Eqs. (61) and (66) provide information on the number of photons scattered from a spherically-focused ultrastrong laser pulse with its angular distribution.

In order to estimate the number of photons scattered from the NBV, the use of fs high-power laser pulses is assumed to induce NBV as shown in Fig. 1. The peak powers for a 4π-spherically-focused laser pulse are assumed to be 10, 100, and 1000 PW. A 30 fs, 10 PW, or 100 PW probe laser pulse propagates through the NBV and is scattered by it. Although these probe pulse powers are high, they are focused conventionally by a parabolic mirror so that the changes to the effects on the NBV by them are much smaller than the 4π-spherically-focused pulse and can be ignored. The parameters for the focused and probe laser pulses used in the following

calculations are summarized in Table I. The differential photon number $\frac{1}{N_p}\frac{dN_S}{d\Omega}$, normalized to the incident probe photon number N_p, is calculated to estimate the scattered photons with these laser beam parameters.

Figure 3 shows the differential photon number for different combinations of laser peak power and wavelength. The peak powers P_{peak} and P_p in the figure mean the peak powers of the 4π-spherically-focused laser and the probe laser pulses, respectively, and the angular frequencies ω and ω_γ are the angular frequencies for the focused laser and the probe laser, respectively. In the calculations, the phase delay (δ_p) between the two laser pulses is assumed to be zero. Figures 3(a) and 3(c) show the differential photon number calculated for three different laser power combinations: 10 (the peak power for

TABLE I. The parameters of laser pulses. In the table, Ti:S and Nd:glass mean the Ti:sapphire and Nd:glass high power laser systems, respectively.

	Peak power (PW)	Center wavelength (μm)	Pulse duration (fs)	Laser system
4π-spherically-focused laser pulse	10	0.8 or 1.05	30 or 150	Ti:S or Nd:glass
	100	0.8 or 1.05	30 or 150	Ti:S or Nd:glass
	1000	0.8	30	Ti:S
Probe laser pulse	10	0.8 or 0.4	30	Ti:S
	100	0.8 or 0.4	30	Ti:S

the focused laser)–10 PW (the peak power for the probe laser) (shortly, 10–10 PW case hereafter) for the blue line, 100–100 PW case for the red line, and 1000–100 PW case for the green line. The peak intensities of the 4π-spherically-focused laser pulse with a wavelength of 0.8 μm become 1.82×10^{25}, 1.82×10^{26}, and 1.82×10^{27} W/cm^2 for 10, 100, and 1000 PW laser pulses, respectively. In case of the probe beam, the peak intensities reach $\sim 5 \times 10^{24}$ and $\sim 5 \times 10^{25}$ W/cm^2 for 10 and 100 PW laser pulses, respectively. When considering the divergence of the probe pulse after focus, the photons scattered within an angle of $\pm\theta_{\text{probe}}$ ($\approx \pm\pi/7.2 \approx \pm 26°$) propagate with the probe pulse, so the detector for measuring the scattered photons should be located in a geometrical shadow

to remove the huge background intensity of the probe beam. The geometrical shadow is determined by the f number of the OAP for the probe beam and, in our case using an f number of 1, it is formed at an angle of $\theta > +26°$ or $\theta < -26°$, so the detector should be located at an angle θ_{det} wider than $\theta = \sim 26°$ (for example, $\theta_{\text{det}} = +30°$ or $\theta_{\text{det}} = -30°$). The differential photon numbers at $\theta = 30°$ and $\phi = 0°$ are calculated to be 2.28×10^{-19} (blue line), 2.28×10^{-17} (red line), and 2.28×10^{-15} (green line) for the x-pol/x-pol scattering case, and to be 2.24×10^{-19} (blue line), 2.24×10^{-17} (red line), and 2.24×10^{-15} (green line) for the x-pol/y-pol scattering case, respectively. This result means that considering the incident photon number ($\sim 1 \times 10^{21}$ for 10 PW, $\sim 1 \times 10^{22}$ for 100 PW
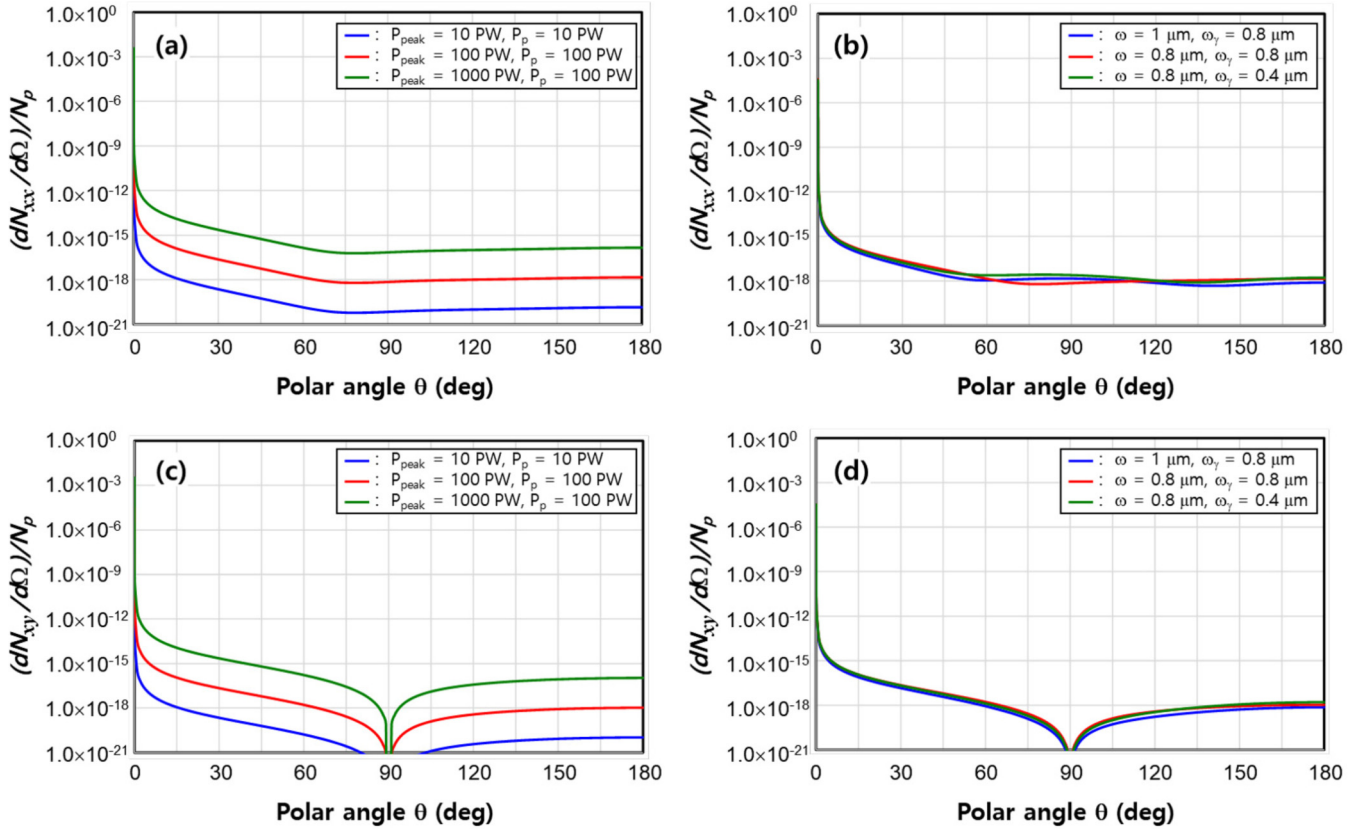

FIG. 3. The differential photon number scattered from a nonlinear birefringent vacuum induced by an ultrastrong laser pulse. P_{peak} and P_p mean laser peak powers of the 4π-spherically-focused laser pulse and the probe laser pulse, respectively. ω and ω_γ means central angular frequencies of the 4π-spherically-focused laser pulse and the probe laser pulse, respectively. (a) The differential photon number for the x-pol/x-pol scattering case at different laser power combinations. (b) The differential photon number for the x-pol/x-pol scattering case depending on the wavelength combination. (c) The differential photon number for the x-pol/y-pol scattering case at different laser power combinations. (d) The differential photon number for the x-pol/y-pol scattering case depending on the wavelength combination.
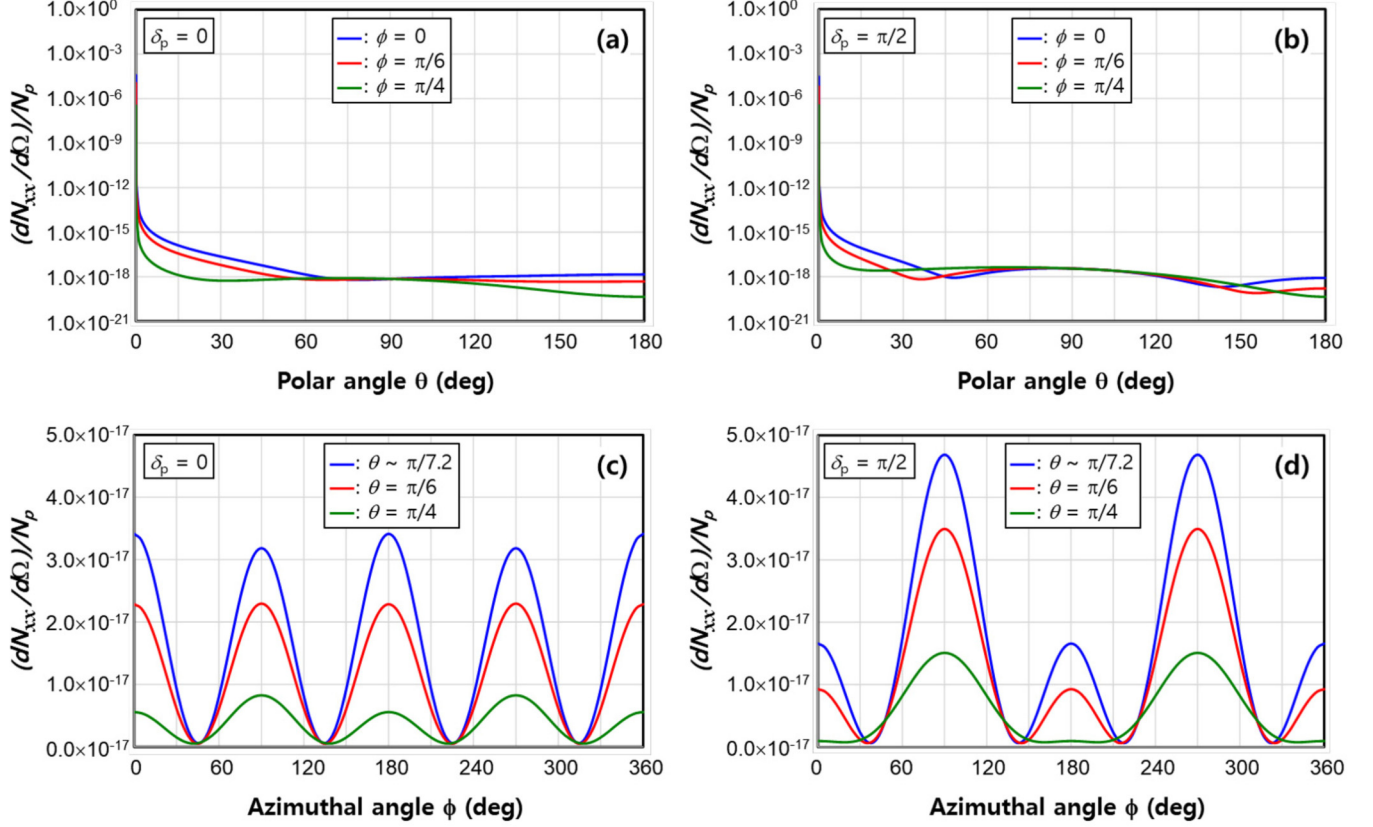
FIG. 4. The angular dependence of the differential photon number for the x-pol/x-pol scattering case at two different phase delays. The phase delay between the 4π-spherically-focused laser pulse and the probe laser pulse is zero for (a) and (c), and $\pi/2$ for (b) and (d).

for the probe pulse), the expected number of scattered photons at the unit solid angle is approximately 240 for the 10–10 PW case, 2.4×10^5 for the 100–100 PW case, and 2.4×10^7 for the 1000–100 PW case. In these cases, the center wavelengths of the laser pulses are assumed to be 0.8 μm, which is the typical wavelength of the Ti:sapphire laser.

The dependence of the differential photon number on the wavelength combination is shown in Figs. 3(b) and 3(d). In the calculations, the use of 100 PW power is assumed for both the focused and probe laser pulses. Three different wavelength combinations, such as 1 μm wavelength (the focused laser) and 0.8 μm wavelength (the probe laser) (shortly, 1–0.8 μm case hereafter) for the blue line, 0.8–0.8 μm case for the red line, and 0.8–0.4 μm case for the green line, are investigated at a polar angle of $\theta = 30°$. For the x-pol/x-pol scattering case, the normalized photon number increases from 1.10×10^{-17} for the 1–0.8 μm scattering case to 2.28×10^{-17} for the 0.8–0.8 μm scattering case. And, for the x-pol/y-pol scattering case, the 0.8–0.8 μm scattering case shows the greatest differential photon number of 2.24×10^{-17}.

Figures 4 and 5 show the dependence of the differential photon number on the azimuthal angle ϕ and the phase delay δ_p. Two different conditions ($\delta_p = 0$ and $\delta_p = \pi/2$) for the phase delay are shown in the figures. The 0.8–0.8 μm scattering case is considered for the 100–100 PW scattering case. The greatest differential photon number of 3.50×10^{-17} can be obtained for the x-pol/x-pol scattering under conditions of $\phi = \pi/2$ and $\delta_p = \pi/2$ at $\theta = \pi/6$. This differential

photon number increases to 3.50×10^{-15} for the 1000–100 PW scattering case.

This result means that for the 1000–100 PW laser pulse scattering case the maximum number ($dN_S/d\Omega$) of scattered photons of 3.52×10^7 is expected for the unit solid angle. Given a detector size of 1 cm by 1 cm located 1 m away from the interaction point (focus), a total number of about 154 photons can be expected on the detector. A single photon counting technique can be used to detect the scattered photons. The expected number of scattered photons calculated with this approach seems much higher than that calculated with the photon-photon scattering approach based on QED [57]. For example, in our calculation, the number ($dN_{xx}/d\Omega$) of scattered photons at a specific solid angle is expected to be more than 6000 [Fig. 3(a)] when two 100 PW laser pulses are used for the focused and the probe pulses, yielding the incident number (N_p) of the probe photon number as $\sim 1 \times 10^{22}$. Under the same condition, the number of scattering events is expected to be $\sim 1 \times 10^{-12}$ for the conventional approach [56,57] based on the QED calculation. Comparing Eqs. (61) and (66) to Eq. (3) in [56], the major difference between the two expressions comes from the number of probe photons N_p in Eqs. (61) and (66). According to [58], the different number of scattered photons between the two calculations is related to the calculation of the luminosity for the coherent photons. In their explanation, for fermion, the luminosity can be calculated by $N^2/\pi r^2$ (Eq. (5.1) in [58]), where N is the total fermion number contained in the bunch and r is the radius
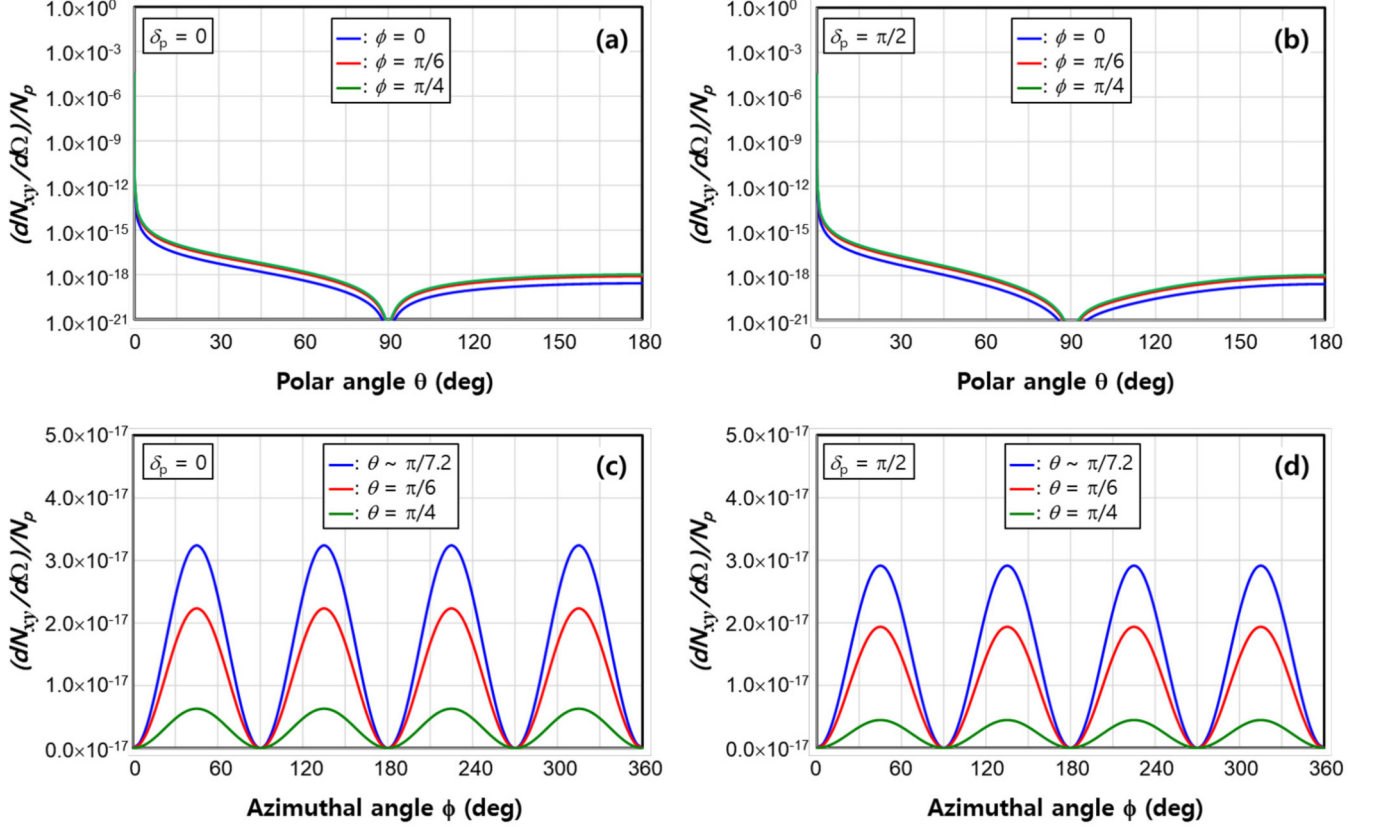
FIG. 5. The angular dependence of the differential photon number for the x-pol/y-pol scattering case at two different phase delays. The phase delay between the 4π-spherically-focused laser pulse and the probe laser pulse is zero for (a) and (c), and $\pi/2$ for (b) and (d).

of the bunch. However, for coherent photons, the number of scattered photons based on the luminosity calculation should be proportional to N^3, assuming the same number N of the probe beam as the focused beam, and the required number of probe photons for a single photon scattered is $\sim 10^{21}$. When two coherent photon beams have different photon numbers (i.e., N and N_{probe}), the proportionality of the scattered photon number can be modified as $N^2 N_{\text{probe}}$. In our case, the photons are in coherent states because the mathematical expression describing the temporal distribution of a femtosecond laser pulse in Eq. (23),

$$e^{-\frac{(t-t_d)^2}{2\Delta t_p^2}} e^{-i\omega t}, \tag{68}$$

follows the general expression for the wave function of a squeezed coherent state. And their estimation agrees well with our calculation results. Another approach [22,57,59] based on the four-wave interaction of intense radiation using three incoming photon beams also shows the same dependency (N^3) on the number N of photons in each photon beam as our results. Thus, careful examination for understanding the discrepancy and agreement on the number of scattered photons between different approaches is needed and a more comprehensive explanation should be addressed in other publications.

In summary, the calculation shows that a detectable number of photons can be scattered from the NBV induced by an exawatt (EW, 1000 PW) power laser facility, which will be available in the near future. All the results can be used to de-

tect the scattered photons from the NBV induced by ultrashort ultrastrong laser pulses. In the experimental measurement of photons scattered from the vacuum, there will be other photons emitted/scattered from particles (atoms or gas molecules even under a high vacuum condition) within the interaction region. Thus, the suppression of photons emitted/scattered from particles will be a big challenge in purely detecting photons scattered from the nonlinear vacuum.

IV. CONCLUSION

The light scattering from the NBV induced by a 4π-spherically-focused fs high-power laser pulse has been investigated through the Lagrangian formalism and the perturbation method using the Born approximation. The electric permittivity and magnetic permeability tensors are explicitly expressed for the NBV when the fs high-power laser pulse is 4π-spherically-focused. The NBV is modeled as a scattering potential for calculating the scattered electric fields through the Born approximation. The mathematical expressions of the differential scattering cross sections for x-pol/x-pol and x-pol/y-pol scatterings are derived. The number of photons scattered by the NBV has been calculated in the laser power range of 10 to 1000 PW, which will be available in the near future. The calculation shows that a total number of >150 photons can be measured on a detector with a size of 1 cm by 1 cm located 1 m away from the focus of an EW laser pulse.

[1] J. H. Sung, S. K. Lee, T. J. Yu, T. M. Jeong, and J. Lee, Opt. Lett. **35**, 3021 (2010).

[2] ELI-beamlines, http://www.extreme-light-infrastructure.eu/.

[3] XCELS, http://www.xcels.iapras.ru/.

[4] SULF, http://english.siom.cas.cn/.

[5] G. A. Mourou, T. Tajima, and S. V. Bulanov, Rev. Mod. Phys. **78**, 309 (2006).

[6] A. DiPiazza, C. Muller, K. Z. Hatsagortsyan, and C. H. Keitel, Rev. Mod. Phys. **84**, 1177 (2012).

[7] J. Schwinger, Phys. Rev. **82**, 664 (1951).

[8] J. J. Klein and B. P. Nigam, Phys. Rev. **135**, B1279 (1964).

[9] S. L. Adler, Ann. Phys. **67**, 599 (1971).

[10] M. Marklund and P. K. Shukla, Rev. Mod. Phys. **78**, 591 (2006).

[11] W. Heisenberg and H. Euler, Z. Phys. **98**, 714 (1936).

[12] G. V. Dunne, *Heisenberg-Euler Effective Lagrangians: Basics and Extensions, from Fields to Strings: Circumnavigating Theoretical Physics* (World Scientific, Singapore, 2005).

[13] R. Karplus and M. Neuman, Phys. Rev. **80**, 380 (1950).

[14] R. Karplus and M. Neuman, Phys. Rev. **83**, 776 (1951).

[15] B. D. Tollis, Nuovo Cim. **35**, 1182 (1965).

[16] R. Cameron, G. Cantatore, A. C. Melissinos, G. Ruoso, Y. Semertzidis, H. J. Halama, D. M. Lazarus, A. G. Prodell, F. Nezrick, C. Rizzo, and E. Zavattini, Phys. Rev. D **47**, 3707 (1993).

[17] F. D. Valle, A. Ejlli, U. Gastaldi, G. Messineo, E. Milotti, R. Pengo, G. Ruoso, and G. Zavattini, Eur. Phys. J. C **76**, 24 (2016).

[18] ATLAS collaboration, Nat. Phys. **13**, 852 (2017).

[19] ATLAS collaboration, Phys. Rev. Lett. **123**, 052001 (2019).

[20] K. Homma, K. Matsuura, and K. Nakajima, Prog. Theor. Exp. Phys. **2016**, 013C01 (2016).

[21] T. Inada, T. Yamazaki, T. Namba, S. Asai, T. Kobayashi, K. Tamasaku, Y. Tanaka, Y. Inubushi, K. Sawada, M. Yabashi, T. Ishikawa, A. Matsuo, K. Kawaguchi, K. Kindo, and H. Nojiri, Phys. Rev. Lett. **118**, 071803 (2017).

[22] B. King, H. Hu, and B. Shen, Phys. Rev. A **98**, 023817 (2018).

[23] lightsoources.org, https://lightsources.org/lightsources-of-the-world/.

[24] I. J. Kim, K. H. Pae, C. M. Kim, H. T. Kim, H. Yun, S. J. Yun, J. H. Sung, S. K. Lee, J. W. Yoon, T. J. Yu, T. M. Jeong, C. H. Nam, and J. Lee, Nat. Commun. **3**, 1231 (2012).

[25] S. V. Bulanov, T. Z. Esirkepov, M. Kando, A. S. Pirozhkov, and N. N. Rosanov, Phys. Usp. **56**, 429 (2013).

[26] N. D. Powers, I. Ghebregziabher, G. Golovin, C. Liu, S. Chen, S. Banerjee, J. Zhang, and D. P. Umstadter, Nat. Photon. **8**, 28 (2014).

[27] J. Koga, S. V. Bulanov, T. Esirkepov, M. Kando, S. S. Bulanov, and A. Pirozhkov, Plasma Phys. Control. Fusion **60**, 074007 (2018).

[28] J. Mu, T. Z. Esirkepov, P. Valenta, T. M. Jeong, Y. Gu, J. K. Koga, A. S. Pirozhkov, M. Kando, G. Korn, and S. V. Bulanov, Phys. Wave Phenom. **27**, 247 (2019).

[29] E. Lundstrom, G. Brodin, J. Lundin, M. Marklund, R. Bingham, J. Collier, J. T. Mendonca, and P. Norreys, Phys. Rev. Lett. **96**, 083602 (2006).

[30] S. S. Bulanov, V. D. Mur, N. B. Narozhny, J. Nees, and V. S. Popov, Phys. Rev. Lett. **104**, 2204040 (2010).

[31] S. V. Bulanov, T. Esirkepov, and T. Tajima, Phys. Rev. Lett. **91**, 085001 (2003).

[32] S. S. Bulanov, T. Z. Esirkepov, A. G. R. Thomas, J. K. Koga, and S. V. Bulanov, Phys. Rev. Lett. **105**, 220407 (2010).

[33] S. S. Bulanov, A. Maksimchuk, A. G. Zhidkov, C. Schroeder, E. Esarey, and W. P. Leemans, Phys. Plasmas **19**, 020702 (2012).

[34] I. Gonoskov, A. Aiello, S. Heugel, and G. Leuchs, Phys. Rev. A **86**, 053836 (2012).

[35] T. M. Jeong, S. Weber, B. L. Garrec, D. Margarone, T. Mocek, and G. Korn, Opt. Express **23**, 11641 (2015).

[36] T. M. Jeong, S. V. Bulanov, S. Weber, and G. Korn, Opt. Express **26**, 33091 (2018).

[37] T. M. Jeong, S. V. Bulanov, P. Sasorov, S. S. Bulanov, J. K. Koga, and G. Korn, Opt. Express **28**, 13991 (2020).

[38] Y. Monden and R. Kodama, Phys. Rev. Lett. **107**, 073602 (2011).

[39] Y. Monden and R. Kodama, Phys. Rev. A **86**, 033810 (2012).

[40] T. G. Brown, Unconventional polarization states: Beam propagation, focusing, and imaging, in *Progress in Optics*, edited by E. Wolf (Elsevier, London, 2011), Vol. 56, p. 81.

[41] T. M. Jeong, S. V. Bulanov, W. Yan, S. Weber, and G. Korn, OSA Continuum **2**, 2718 (2019).

[42] M. Born and E. Wolf, *Principles of Optics* (Cambridge University Press, Cambridge, 2003).

[43] V. B. Berestetskii, E. M. Lifshitz, and L. P. Pitaevskii, *Quantum Electrodynamics* (Pergamon, New York, 1982).

[44] N. B. Narozhny, S. S. Bulanov, V. D. Mur, and V. S. Popov, Phys. Lett. A **330**, 1 (2004).

[45] V. I. Ritus, J. Sov. Laser Res. **6**, 497 (1985).

[46] A. DiPiazza, M. Tamburini, S. Meuren, and C. H. Keitel, Phys. Rev. A **98**, 012134 (2018).

[47] V. Dinu, T. Heinzl, A. Ilderton, M. Marklund, and G. Torgrimsson, Phys. Rev. D **89**, 125003 (2014).

[48] T. G. Blackburn, D. Seipt, S.-S. Bulanov, and M. Marklund, Phys. Plasma **25**, 083108 (2018).

[49] I. A. Aleksandrov, G. Plunien, and V. M. Shabaev, Phys. Rev. D **99**, 016020 (2019).

[50] A. Ilderton, B. King, and D. Seipt, Phys. Rev. A **99**, 042121 (2019).

[51] W. Dittrich and H. Gies, Phys. Rev. D **58**, 025004 (1998).

[52] Y. E. Geints, A. M. Kabanov, A. A. Zemlyanov, E. E. Bykova, O. A. Bukin, and S. S. Golik, Appl. Phys. Lett. **99**, 181114 (2011).

[53] Z. W. Wilkes, S. Varma, Y.-H. Chen, H. M. Milchberg, T. G. Jones, and A. Ting, Appl. Phys. Lett. **94**, 211102 (2009).

[54] I. S. Gradshteyn and I. M. Ryzhik, *Table of Integrals, Series, and Products* (Academic, New York, 2007).

[55] N. B. Narozhnyi, J. Exp. Theor. Phys. **28**, 371 (1969).

[56] H. Kadlecova, G. Korn, and S. V. Bulanov, Phys. Rev. D **99**, 036002 (2019).

[57] J. K. Koga, S. V. Bulanov, T. Z. Esirkepov, A. S. Pirozhkov, M. Kando, and N. N. Rosanov, Phys. Rev. A **86**, 053823 (2012).

[58] Y. Fujii and K. Homma, Prog. Theor. Phys. **126**, 531 (2011).

[59] N. N. Rosanov, Zh. Eksp. Teor. Fiz. **103**, 1996 (1993) [Sov. Phys. JETP **76**, 991 (1993)].